CI&CEQ
Chemical Industry & Chemical Engineering Quarterly

Available online at
Association of the Chemical Engineers of Serbia AChE
www.ache.org.rs/CICEQ

Chem. Ind. Chem. Eng. Q. 29 (1) 53–59 (2023) CI&CEQ

LV CHAO[1,2]
YIN HONGXIN[2]
SUN MINGHE[2]
ZHU HANGYU[1]

[1]Key Laboratory for Ferrous Metallurgy and Resources Utilization of Ministry of Education, Wuhan University of Science and Technology, Wuhan, China

[2]School of Control Engineering, Northeastern University at Qinhuangdao, Hebei, China

SCIENTIFIC PAPER

UDC 66.092-977:54

SIMULATION STUDY OF CITRIC ACID EFFECTS ON PYROLYSIS OF HYDROCHLORIC ACID PICKLING WASTE LIQUOR

Article Highlights

- The couples and simulations of fluid flow, phase change, and chemical reactions are achieved
- New chemical reactions are added, describing the phenomenon of Fe_3O_4 appearance
- The effects of citric acid on the ingredient of reaction products are discussed

Abstract

During pyrolysis of hydrochloric acid pickling waste liquid in a Venturi reactor from iron and steel enterprises, the reaction products agglomerated and hindered product recovery. Addition of citric acid to materials at the inlet improved product distribution. In this paper, a numerical simulation of the combustion, phase change, and gas-solid chemistry involved in a citric acid-added pickling waste liquid was conducted. These results showed that citric acid added to the inlet resulted in a peak concentration of carbon dioxide (CO_2) in the back half of the Venturi throat, and some ferric oxide (Fe_2O_3) underwent a secondary reaction to afford ferroferric oxide (Fe_3O_4). As the addition of citric acid increased, the flow of Fe_2O_3 at the outlet first increased and then decreased, while the flow rate of Fe_3O_4 first decreased and then increased. When the ratio of citric acid was 7%, the flow rate of Fe_2O_3 was the smallest, and the flow rate of Fe_3O_4 was the largest.

Keywords: pyrolysis, citric acid, Fe_2O_3, Fe_3O_4, numerical simulation.

Hydrochloric acid is used during steel production to remove oxides from the product surface, resulting in a great deal of pickling waste liquid [1]. Most steel manufacturers use Ruthner spray atomization roasting to regenerate hydrochloric acid, which results in an iron oxide powder by-product [2]. The Fe_2O_3 by-product can be used in pigments, polishing powders, and catalysts [3–5]. Also, Fe3O4 can be used in magnetic materials and the manufacture of telecommunications equipment [6,7]. However, this process line requires high capital costs and regular cleaning and replacement of atomizing nozzles, which are difficult for small and medium-sized companies to achieve. Small and medium-sized companies use lime and calcium carbide slag, among other things, to neutralize the reaction, and the pH of the waste liquid is adjusted and discharged directly, which results in a waste of resources and the formation of solid waste [8]. Therefore, developing new low-cost treatment options for pickling waste liquid is important. Using a Venturi reactor for waste acid recycling effectively reduces equipment costs, efficiently recovers by-products, and promotes the process.

Many scholars have studied the spray pyrolysis technique. For the preparation of MgO by spray pyrolysis of bischofite in salt lakes, Liu *et al.* [9] used computational fluid dynamics (CFD) to simulate the spray pressure and temperature distribution of the pyrolysis furnace; this provided data and the model basis for nozzle selection, pyrolysis furnace structure optimization and flow field study. Shammari *et al.* [10] used spray pyrolysis to successfully prepare TiO_2/reduced graphene oxide (rGO) films with different

Correspondence: Z. Hangyu, Key Laboratory for Ferrous Metallurgy and Resources Utilization of Ministry of Education, Wuhan University of Science and Technology, Wuhan, 430081, Hubei, P.R. China.
E-mail: zhuhy@wust.edu.cn; lvchao@neuq.edu.cn
Paper received: 3 October, 2021
Paper revised: 14 April 2022
Paper accepted: 7 July, 2022

https://doi.org/10.2298/CICEQ211003013C

GO concentrations (0, 3, 5, and 10 wt.%) on fluorine-doped tin oxide (FTO) glass substrates. TiO_2/rGO thin films prepared from different GO concentrations (0, 3, 5, and 10 wt.%) were deposited on fluorine-doped tin oxide (FTO) glass substrates using a spray pyrolysis technique (SPT). Moumen *et al.* [11] used spray pyrolysis to prepare CuO films and discussed the influence of substrate temperature on the structure and optical properties of CuO films deposited using spray pyrolysis. The effect of substrate temperature on the structural and optical properties of the films was discussed. Lv *et al.* [12–14] proposed a new process for preparing metal oxides by direct pyrolysis of a solution containing a rare earth chloride, magnesium chloride, and pickling waste hydrochloric acid. This process incorporated a Venturi reactor that atomized the solution using the heat generated by the combustion of methane to provide energy for the phase change of the solution and the pyrolysis of the metal chloride solution to obtain high-quality metal oxides. The structure of the Venturi reactor contributes to a sharp increase in gas velocity at the throat. Then the solution was fiercely collided into droplets by the high-speed gas, which can enhance the mixing and increase the reaction efficiency. Particle agglomerations and large particle sizes were observed when the Venturi reactor was used. Citric acid was added to change the physical properties of the metal chloride solution to solve this problem by eliminating the hollowing and agglomeration of the product particles [15].

Citric acid may also be added to $FeCl_2$ and $FeCl_3$ solutions to improve Fe_2O_3 agglomeration in a Venturi reactor. In this paper, the direct pyrolysis of pickling waste liquid after citric acid addition was simulated and studied; the coupling of combustion, phase transition, and gas-solid chemistry was completed using Fluent software combined with a user-defined function (UDF).

MODELLING

Figure 1 shows the dimensions of the reactor; the length was 0.85 m, the left-hand gas-phase inlets consisted of a fuel inlet (inlet1), an oxygen inlet (inlet 2), and pipe diameters of Φ1 = 0.01 m and Φ2 = 0.02 m. The sectional diameter of the material inlet (inlet 3) was d = Φ1 = 0.01 m. The sectional diameters of the straight pipelines were d_1 = d_2 = 0.05 m. The lengths of the straight pipelines in front and behind the throat were L_3 = 0.15 and L_4 = 0.3 m, respectively. The throat diameter was d_e = d_1/2 = 0.025 m, length (4*d_e) = 0.1 m; the length of the diameter-variable pipeline was L_1 = L_2 = 0.14 m (tan 8° < [0.5* (d_1-d_e)/L_1] <tan 20°), L_5 = 0.02 m. The sectional diameter of the outlet was 0.05 m. We chose a grid division of 230k in the simulations.

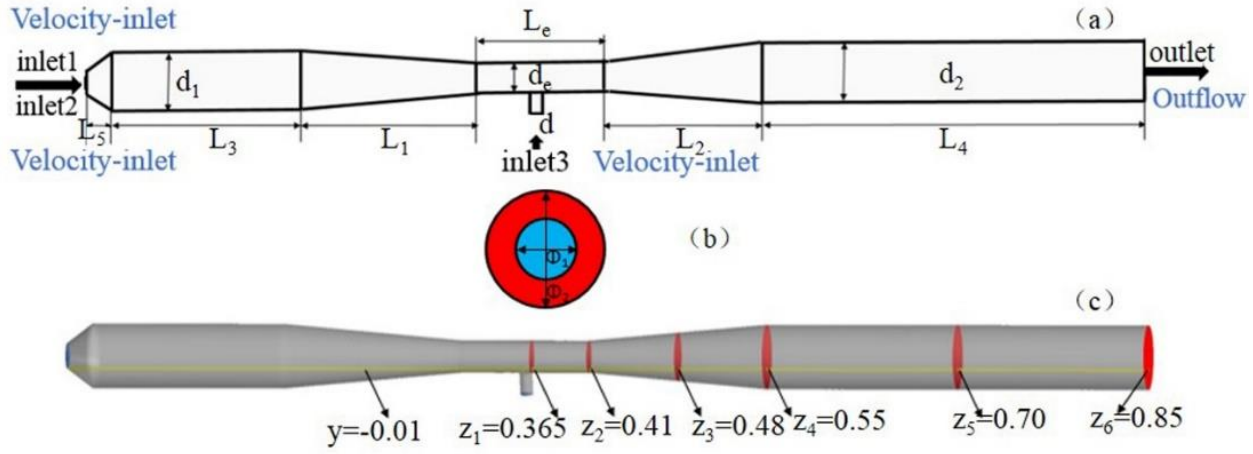

Figure 1. Jet-flow pyrolysis reactor (a) dimension (b) section of gas-phase inlet (c) monitoring line and monitoring surface.

ANSYS 14.5 software was used for the numerical simulation. The simulations were based on a 3D non-steady algorithm, an Euler multi-phase flow model, and volume-finite discrete differential equations. The control equations were differentially treated using a second-order upwind scheme; all items converged to 10^{-4} except for energy (to 10^{-6}). This study focused on $FeCl_2$ and $FeCl_3$ pyrolysis inside the reactor, and the main reactions included:

$$H_2O(l) \rightarrow H_2O(g) \quad (1)$$

$$HCl(l) \rightarrow HCl(g) \quad (2)$$

$$CH_4(g) + 2O_2(g) \rightarrow CO_2(g) + 2H_2O(g) \quad (3)$$

$$2FeCl_2(s) + 2H_2O(g) + 1/2O_2(g) \rightarrow Fe_2O_3(s) + 4HCl(g) \quad (4)$$

$$2FeCl_3(s) + 3H_2O(g) \rightarrow 2Fe_2O_3(s) + 6HCl(g) \quad (5)$$

$$2C_6H_8O_7 + 9O_2(g) \rightarrow 12CO_2(s) + 8H_2O(g) \quad (6)$$

$$6Fe_2O_3(s) \rightarrow 4Fe_3O_4(s) + O_2(g) \quad (7)$$

We used UDFs to simulate these processes, employing the boundary conditions summarized in Table 1 and CH_4, O_2, CO_2, HCl(g), H_2O(g), HCl(l), H_2O(l), $FeCl_2$, $FeCl_3$ and Fe_2O_3 as the chemical species involved in the reactions. The physical parameters of all substances were identified by searching inorganic thermodynamics manuals [16]; the particle sizes of Fe_2O_3 and Fe_3O_4 were up to 1 μm. $C_6H_8O_7$ was customized according to its physical properties. The boundary conditions are shown in Table 1.

Table 1. Boundary conditions

	CH_4 inlet	O_2 inlet	Material inlet	Outlet
Condition	Velocity-inlet	Velocity-inlet	Velocity-inlet	Outflow
Value (m/s)	2.88	31.73	0.015 (10% $FeCl_2$, 10% $FeCl_2$, 5% HCl)	
Value (m/s)	2.88	31.73	0.015 (10% $FeCl_2$, 10% $FeCl_2$, 5% HCl, 5%–9% $C_6H_8O_7$)	

RESULTS AND DISCUSSION

Result validation

The mass flow rate at the outlet of the Venturi reactor maintained steady when the simulated time reached 60 s. As shown in Figure 2, when comparing the flow rates of HCl, Fe_2O_3, and Fe_3O_4 collected at the outlet, the numerical simulation exceeds the experimental physical value, which is caused by the loss of the mixed solution and measurement errors caused by the recovery process. However, the error between the simulation and the experiment results was below 5%, so the model and boundary condition settings for the numerical simulation are accurate.

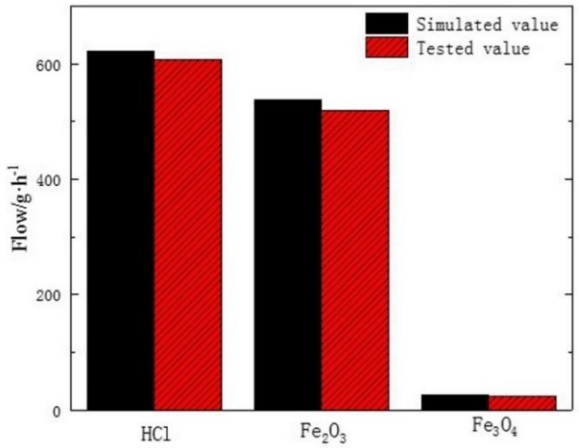

Figure 2. Comparison of product results at the outlet.

Velocity, temperature, and distribution of component concentrations

Figure 3(a) shows the velocity cloud diagram and a velocity vector diagram of the gas phase. Figure 3(a) shows the gas phase velocity maximized at the oxygen inlet and the Venturi throat. Starting from the Venturi throat, a low-velocity area appears in the lower part of the reactor. Figure 3(b) shows the velocity cloud diagram and velocity of the solid phase. Figure 3(b) also indicates the solid phase reached a maximum velocity at the upper right side of the throat. A low-velocity region appears in the lower part of the reactor at the back of the throat due to the vertical collision of the gas and solid phases.

Figure 4 shows the temperature distribution cloud diagrams in the Venturi reactor. The reactor's internal temperature exceeded 2000 K and sufficed for water and hydrochloric acid evaporation from $FeCl_2$ and $FeCl_3$ solutions and pyrolysis. The combustion of methane generated the temperature; the high-temperature zone was concentrated in the first half of the reactor, and the low-temperature zone appeared at the material inlet. The temperature distribution differed from a previous literature report [15] due to a much higher oxygen flow rate.

Figure 5 shows a cloud diagram of the concentration distribution for each component in a

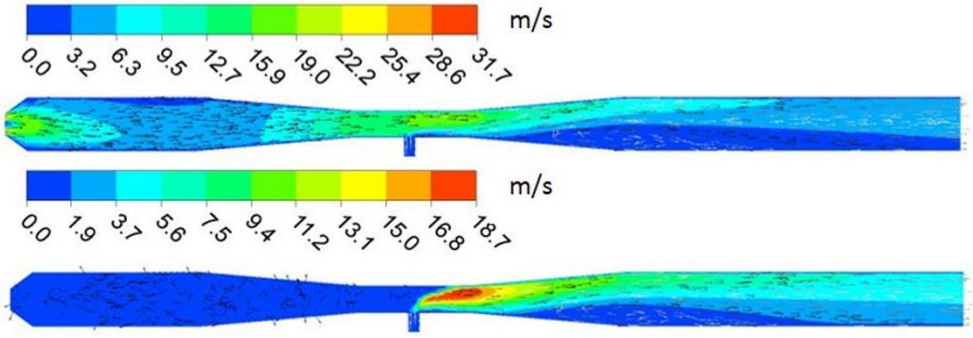

Figure 3. Velocity field distributions.

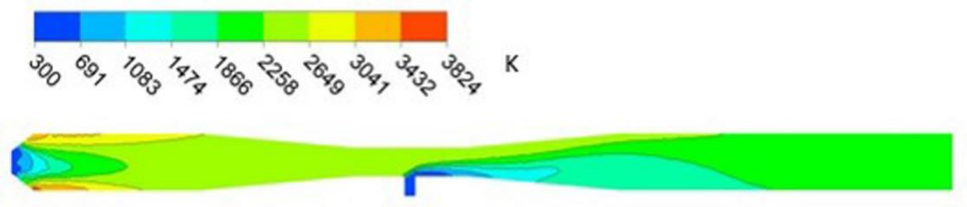

Figure 4. Temperature field distribution.

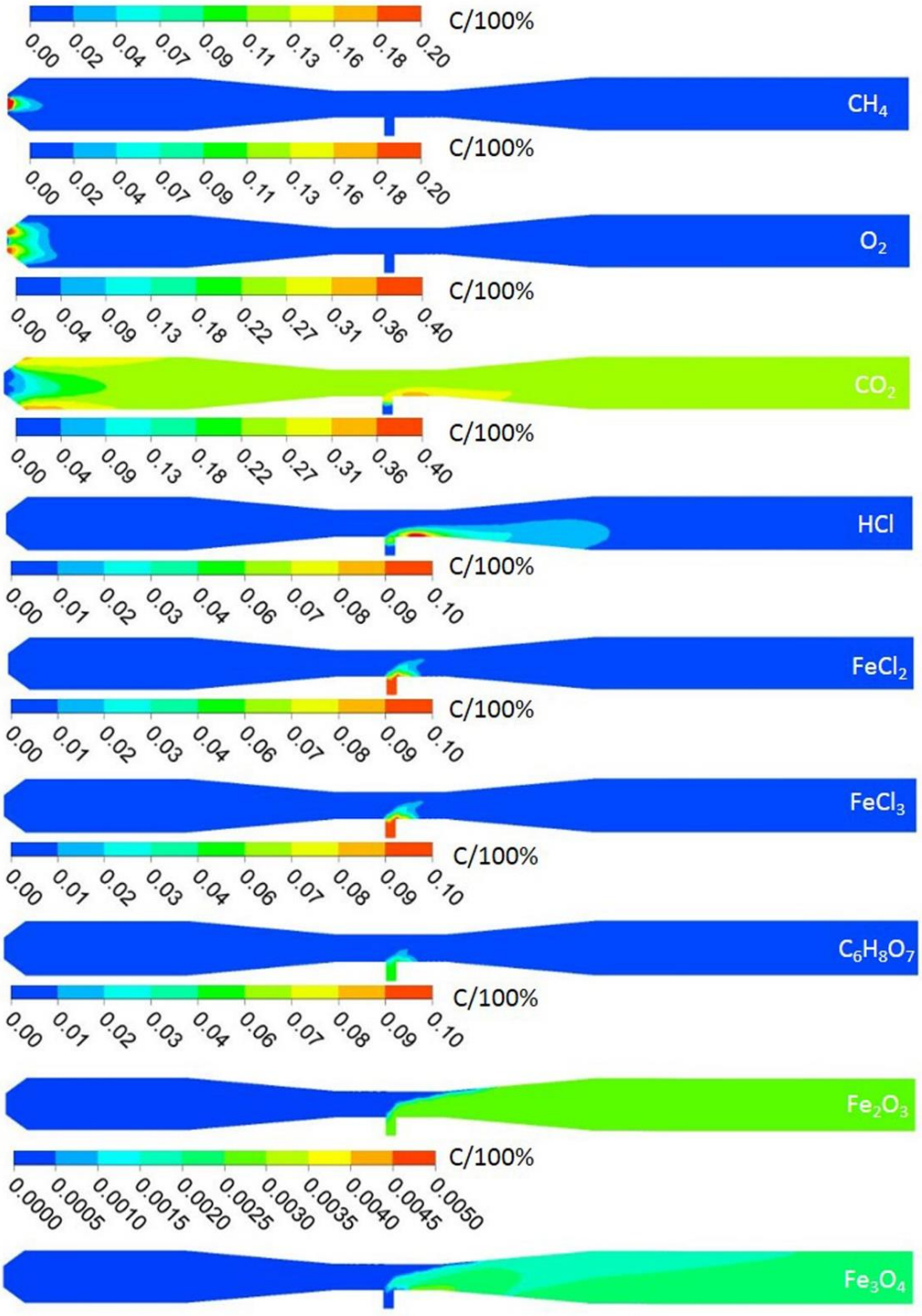

Figure 5. Distribution of component concentrations.

Venturi reactor and methane concentrated primarily at the methane inlet. As the combustion reaction progressed, methane reacted completely, and the concentration dropped to zero. Oxygen concentrated mainly at the oxygen inlet, and most of the oxygen reacted as combustion progressed. The oxygen produced by Eq. (7) will participate in the chemical reaction according to Eqs. (6) and (4). Therefore, the residual oxygen content was too low obviously in the throat. Carbon dioxide was produced and accumulated with the addition of CO_2 generated by the pyrolysis of citric acid at the Venturi throat; this resulted in a high CO_2 concentration distribution area at the rear of the throat. Evaporation from the hydrochloric acid solution and pyrolysis of cerium chloride produced hydrogen chloride and reached its peak concentration in the latter half of the Venturi throat. The high concentration area of $FeCl_2$, $FeCl_3$, and $C_6H_8O_7$ was concentrated mainly at the inlet. As pyrolysis continued, $FeCl_2$, $FeCl_3$, $C_6H_8O_7$ completely reacted, and their concentrations dropped to zero. Pyrolysis produced Fe_2O_3 and was distributed primarily in the second part of the Venturi reactor. After citric acid addition, Fe_3O_4 was present in the Venturi reactor, albeit at low levels, and indicated that only part of Fe_2O_3 underwent a secondary reaction during pyrolysis. The density of Fe_3O_4 was higher than Fe_2O_3, and that high concentration was localized in the lower part of the pipe.

The concentration changes of CO_2, Fe_2O_3, and Fe_3O_4 on the monitoring line were investigated to analyze the product distributions in the reactor further. Figure 6 shows that CO_2 was produced as combustion of methane proceeded and accumulated with CO_2 generated by $C_6H_8O_7$ decomposition. The concentration of CO_2 at the throat of the Venturi increased rapidly and maximized before decreasing and finally leveling off. The distribution of CO_2 concentrations on the monitoring line was higher than in a previous report [15] because the oxygen velocity was higher, and the high CO_2 concentration area was localized near the reactor wall. After citric acid addition, some Fe_2O_3 in the Venturi reactor reacted to afford Fe_3O_4; however, the total number of Fe ions in the product remained unchanged from the Fe ions added to the material inlet. Therefore, the concentrations of $FeCl_2$ and $FeCl_3$ at the material inlet were consistent with the literature values [15]. Also, the total amount of Fe ions in Fe_2O_3 and Fe_3O_4 agreed with previous literature values [15].

Effects of citric acid levels

Figure 7(a) shows that flow rates of Fe_2O_3 and Fe_3O_4 increased when the reactor was closer to the outlet. Changing the amount of $C_6H_8O_7$ added affected the flow ratio of Fe_2O_3 and Fe_3O_4. Adding 7% $C_6H_8O_7$ resulted in the highest Fe_3O_4 flow rate. As seen in Figure 7(b), increasing citric acid levels caused the flow rate of Fe_2O_3 to increase then decrease; however, the flow rate of Fe_3O_4 initially decreases then increases, and the total Fe ion levels at the outlet remained unchanged. When citric acid levels were 7%, the flow rate of Fe_2O_3 was minimum, and the flow rate of Fe_3O_4 was maximum.

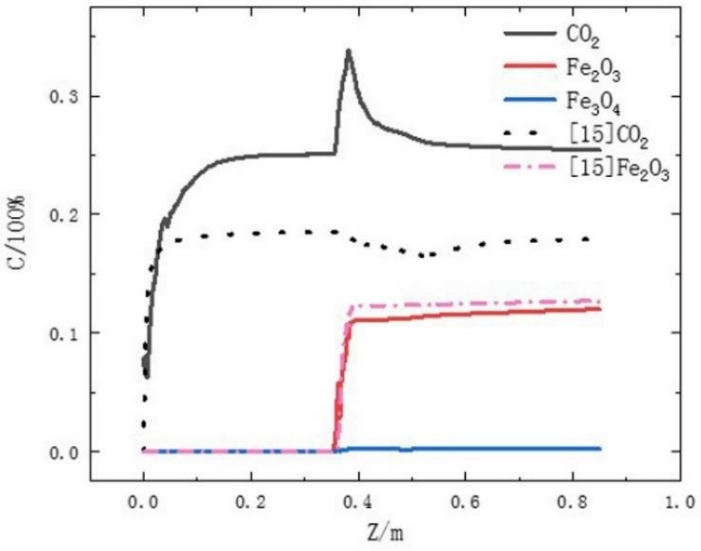

Figure 6. Concentration distribution on the monitoring line.

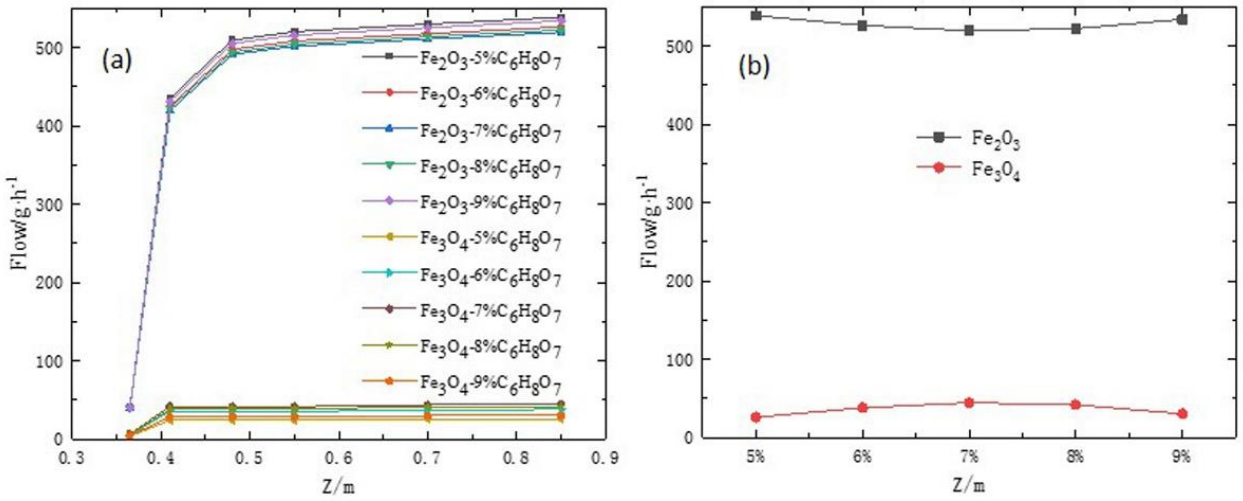

Figure 7. The relationship between the amount of citric acid added and the product (a) at different positions (b) at the outlet.

CONCLUSION

When citric acid was added to the inlet, CO_2 produced by pyrolysis of citric acid and methane combustion combined, and the peak concentration was reached in the back half of the Venturi throat. With the addition of citric acid, part of the Fe_2O_3 in the Venturi reactor underwent a secondary reaction to afford Fe_3O_4, the density of Fe_3O_4 was higher than Fe_2O_3, and that high concentration was localized in the bottom of the pipe. However, the total amount of Fe ions in the product remained unchanged from the Fe ions added at the inlet. As citric acid levels increased, the flow rate of Fe_2O_3 initially increased and then decreased, while the flow rate of Fe_3O_4 first decreased and then increased. Citric acid levels of 7% resulted in the lowest flow rate for Fe_2O_3 and the highest flow rate for Fe_3O_4.

ACKNOWLEDGMENTS

This research was supported by the National Natural Science Foundation of China (51904069), the open fund of the Key Laboratory of iron and steel metallurgy and resource utilization of Wuhan University of science and technology (FMRU19-1), the Scientific Research Fund project of Northeastern University at Qinhuangdao (XNY201808), the Fundamental Research Funds for the Central Universities (N2223026).

REFERENCES

[1] J. Peng, Y. Zhu, D.F. Zhang, Inor. Chem. Ind. 07 (2019) 81–84.

[2] Y.T. Hong, L. Qiao, X.H. Liu, Mod. Chem. Ind. 01 (2005) 48–50.

[3] A.J. Sushilkumar, B Roberta, L.M. Daniele, F. Daniela, E. Christian, Pigm. Resin. Tech. 04 (2014) 219–227. https://doi.org/10.1108/PRT-07-2013-0057

[4] M. A. Ali, M. M. Uddin, M. N. I. Khan, F.U.Z. Chowdhury, S.M. Hoque, S.I. Liba, Chin. Phy. B. 07 (2017) 377–343. https://doi.org/10.1088/1674-1056/26/7/077501

[5] X. Han, L.L. Wang, L. Wang, X.D. Wang, D.Q. Zhao, J. Chin. Ceram. Soc. 07 (2020) 1097–1106. https://doi.org/10.14062/j.issn.0454-5648.2020.07.20190682

[6] Y. Aylin, V.B. Derman, A. Riza, A.A. Ozgur, A. K. Mine, E. Ugur, M. Carl, H.R.L. Appl. Surf. Sci. 521 (2020) 146332. https://doi.org/10.1016/j.apsusc.2020.146332.

[7] S. Yousefinejad, H. Rasti M. Hajebi, M. Kowsari, S. Sadravi, F. Honarasa, Sens. Actuators, B 247 (2017) 691-696. https://doi.org/10.1016/j.snb.2017.02.145.

[8] C.X. Cui, Coal. Chem. Ind, 11 (2010), 37–38.

[9] Y.T. Liu, F.Z. Liu, W. Du, G.M. Lu, J.G. Yu, J. Mater. Sci. Eng. 6 (2018) 1010-1015.

[10] AlShammari A. S., Halim M.M., Yam F.K., K. N. H. Mohd, Mate. Sci. Semi. Proc, 116 (2020) 1–6. https://doi.org/10.1016/j.mssp.2020.105140

[11] A. Moumen, B. Hartiti, E. Comini, Z.El Khalidi, H.M.M.M. Arachchige, S. Fadili, P. Thevenin, Supe. micr, 127 (2019) 2–10. https://doi.org/10.1016/j.spmi.2018.06.061

[12] Lv, C., Zhang, T. A., and Dou, Z. H., Rare Metals, 12 (2019) 1160–1168. https://doi.org/10.1007/s12598-019-01337-9

[13] C. Lv, T.A. Zhang, Z.H. Dou, Q.Y. Zhao, J. Mate, 5 (2019) 1660–1666. https://doi.org/10.1007/s11837-019-03397-9

[14] C. Lv, J. Mate, 12 (2019) 4944–4949. https://doi.org/10.1007/s12598-019-01337-9

[15] G.S. Yang, X. Bian, L.X. Cui, B. Xie, Y.L. Yao, W.Y. Wu. Chin. Rare. Earths, 01 (2017) 72–78. https://doi.org/10.16533/J.CNKI.15-1099/TF.201701013

[16] D.L. Ye, Beijing: Metallurgical industry press, (1981) 250–257. (in Chinese).

LV CHAO[1,2]
YIN HONGXIN[2]
SUN MINGHE[2]
ZHU HANGYU[1]

[1]Key Laboratory for Ferrous Metallurgy and Resources Utilization of Ministry of Education, Wuhan University of Science and Technology, Wuhan, China

[2]School of Control Engineering, Northeastern University at Qinhuangdao, Hebei, China

NAUČNI RAD

SIMULACIJSKO ISTRAŽIVANJE EFEKATA LIMUNSKE KISELINE NA PIROLIZU OTPADNOG LUGA IZ NAGRIZANJA HLOROVODONIČNOM KISELINOM

Tokom pirolize otpadnog luga iz nagrizanja gvožđa i čelika hlorovodoničnom kiselinom u Venturijevom reaktoru proizvodi reakcije aglomeriraju i ometaju obradu proizvoda. Dodavanje limunske kiseline materijalima na ulazu poboljšalo je distribuciju proizvoda. U ovom radu je sprovedena numerička simulacija sagorevanja, promene faze i hemije gasno-čvrsto vezane za obradu otpadnog luga iz procesa nagrizanja limunskom kiselinom. Ovi rezultati su pokazali da limunska kiselina, dodata na ulazu, dovodi do maksimalne koncentracije CO_2 u drugoj polovini Venturijevog grla, dok je deo Fe_2O_3 je podvrgnut sekundarnoj reakciji u kojoj nastaje Fe_3O_4. Kako se količina dodate limunske kiseline povećava, prinos Fe_2O_3 na izlazu se prvo povećava, a zatim smanjuje, dok se prinos Fe_3O_4 prvo smanjuje, a zatim povećava. Kada je odnos limunske kiseline bio 7%, prinos Fe_2O_3 je bio najmanji, a prinos Fe_3O_4 najveći.

Ključne reči: piroliza, limunska kiselina, Fe_2O_3, Fe_3O_4, numerička simulacija.